

B7–H3 as a Prognostic Biomarker and Therapeutic Target in Pediatric central nervous system Tumors



Uday B. Maachani^{*,1}, Umberto Tosi^{*,1}, David J. Pisapia[†], Sushmita Mukherjee[‡], Christopher S. Marnell^{*}, Julia Voronina^{*}, Daniel Martinez[§], Mariarita Santi[§], Nadia Dahmane^{*}, Zhiping Zhou[¶], Cynthia Hawkins[#] and Mark M. Souweidane^{*,**}

^{*}Department of Neurological Surgery, Weill Cornell Medicine, New York, NY, USA; [†]Department of Pathology, Weill Cornell Medicine, New York, NY, USA; [‡]Department of Biochemistry, Weill Cornell Medicine, New York, NY, USA; [§]Department of Pathology, Children's Hospital of Philadelphia, Philadelphia, PA, USA; [¶]Department of Pediatrics, Memorial Sloan Kettering Cancer Center, New York, NY, USA; [#]Department of Pediatric Laboratory Medicine, The Hospital for Sick Children, Toronto, ON Canada; ^{**}Department of Neurological Surgery, Memorial Sloan Kettering Cancer Center, New York, NY, USA

Abstract

B7–H3 (CD276), a member of the B7 superfamily, is an important factor in downregulating immune responses against tumors. It is also aberrantly expressed in many human malignancies. Beyond immune regulatory roles, its overexpression has been linked to invasive metastatic potential and poor prognosis in patients with cancer. Antibody-dependent cell-mediated cytotoxicity strategies targeting B7–H3 are currently in development, and early-phase clinical trials have shown encouraging preliminary results.

To understand the role of B7–H3 in pediatric central nervous system (CNS) malignancies, a comprehensive panel of primary CNS tumors of childhood was examined by immunohistochemistry for levels and extent of B7–H3 expression. In addition, B7–H3 m-RNA expression status and association with overall survival in various pediatric CNS tumor types was accessed by curating publicly available patient gene expression data sets derived from bioinformatics analysis and visualization platforms (GlioVis).

We demonstrate that B7–H3 is broadly expressed in pediatric glial and nonglial CNS tumors, and its aberrant expression, as determined by immunohistochemical staining intensity, correlates with tumor grade. Moreover, high B7–H3 m-RNA expression is significantly associated with worse survival and could potentially improve prognostication in various brain tumor types of childhood. B7–H3 can be used as a therapeutic target, given its tumor selectivity and the availability of targeted therapeutic agents to this antigen.

Translational Oncology (2020) 13, 365–371

Address all correspondence to: Mark M. Souweidane, MD, Department of Neurological Surgery, Weill Cornell Medical College, 525 East 68th Street, New York, NY 10065, USA. E-mail: mmsouwei@med.cornell.edu

¹Denotes equal contribution.

Received 27 September 2019; Revised 10 November 2019; Accepted 11 November 2019

© 2019 The Authors. Published by Elsevier Inc. on behalf of Neoplasia Press, Inc. This is an open access article under the CC BY-NC-ND license (<http://creativecommons.org/licenses/by-nc-nd/4.0/>).

1936-5233/19

<https://doi.org/10.1016/j.tranon.2019.11.006>

Introduction

B7–H3 (CD276) is a type I transmembrane protein belonging to the B7/CD28 superfamily, an important class of immune checkpoint molecules chiefly expressed on the surface of T and B cells [1,2]. In addition to immune cells, expression of B7–H3 is found in a wide variety of tissues and cell types, including nonimmune resting fibroblasts, endothelial cells, osteoblasts, and amniotic fluid stem cells and is induced on antigen-presenting cells [3–5]. The exact role of B7–H3 is controversial, and the existing literature characterizes the role of B7–H3 as either costimulatory or coinhibitory in T cell–mediated adaptive immunity [6]. Recently, numerous studies have demonstrated aberrant overexpression of B7–H3 on both tumor cells and associated stromal cells in both solid and hematologic malignancies such as melanoma, leukemia, and prostate, breast, ovarian, pancreatic, and colorectal cancers; the majority of B7–H3, however, is found in the cytoplasm rather than on the cell surface [7–15]. Normal tissues demonstrate limited expression of B7–H3; although found in many organs, the cell types expressing B7–H3 remain unclear [6].

In vitro and *in vivo* studies on pancreatic cancer and melanoma have found that inhibiting the expression of B7–H3 with short hairpin RNA (shRNA) decreases cell adhesion to fibronectin and reduces migration and matrigel-based invasion abilities [7,16]. Increased levels of B7–H3 in melanoma correlated with activation of JAK2/STAT3/survivin-dependent pathways, which are known to render cancer cells insensitive to chemotherapy and radiation therapy [11,15,17]. Previous studies with a limited number of patient samples have reported the presence of B7–H3 expression in central nervous system (CNS) tumors including medulloblastoma and adult glioma; the same has occurred in neuroblastoma [18–20]. Recently, efforts have focused on using B7–H3 as a prognostic and survival marker in glioblastoma (GBM) and other gliomas, across various subtypes [21]. Other studies also found it to be related to genes associated with immune response, cell proliferation, and angiogenesis [22,23]. Previously, our group demonstrated B7–H3 immunoreactivity and overexpression in diffuse midline gliomas arising in the pons – diffuse intrinsic pontine glioma (DIPG) – and its overexpression in tumor tissues compared with normal samples [12].

Such expression patterns make B7–H3 an attractive target for immunologic and cell-based therapies. For instance, we have recently demonstrated the safety and feasibility of a convection-enhanced delivery (CED) approach targeting B7–H3 with the radiolabeled monoclonal antibody ¹²⁴I–8H9 in pediatric patients with DIPG [24]. In the present study, we assessed the potential clinical significance of B7–H3 expression as a therapeutic and prognostic target in a comprehensive spectrum of pediatric CNS malignancies by investigating B7–H3 immunoreactivity and RNA expression.

Materials and Methods

Patients and Specimens

Pediatric CNS tissue microarrays including astrocytomas, atypical teratoid rhabdoid tumors (AT/RTs), ependymomas, CNS embryonal tumors (CETs), medulloblastomas, meningiomas, germ cell tumors, choroid plexus tumors (CPTs), and craniopharyngiomas were generated at the Department of Pathology at the Children's Hospital of Philadelphia (CHOP) and the Department of Laboratory Medicine & Pathobiology at the Hospital for Sick Children, Toronto, ON, Canada, in accordance with and subject to the approval by the respective ethics committees and institutional review boards. Tumor phenotypes included all major categories of primary CNS tumors of childhood (Table 1). Specimens had been initially obtained either by surgical biopsy or at autopsy from patients with clinicopathologically established diagnoses. TMAs were constructed as previously described [25,26]. We note that age and sex demographics were not available for ependymoma specimens.

B7–H3 Immunohistochemistry and Image Analysis

Tumor B7–H3 expression was assessed by immunohistochemistry, with human lymph nodes serving as a positive control and rodent tissue as a negative control. Briefly, 4- μ m-thick formalin-fixed sections were immunohistochemically stained for B7–H3 with antibody SP206 (1:200, OriGene Technologies) using the Leica Bond Rx automated system (Leica Biosystems, USA). The Bond Refine polymer staining kit (Leica Biosystems) was used, and antigen retrieval was performed with E2 (Leica Biosystems) retrieval solution for 20 min. Individual B7–H3 immunostained (DAB peroxidase)

Table 1. Scoring of B7–H3 immunostaining intensity across tumor types

Tumor type	Positivity	Staining Intensity		
		Low	Medium	High
ATRT	13/13 (100%)	0/13 (0%)	1/13 (8%)	12/13 (92%)
Ependymoma	24/24 (100%)	0/24 (0%)	9/24 (38%)	15/24 (62%)
Medulloblastoma	33/33 (100%)	1/33 (3%)	15/33 (45%)	17/33 (52%)
CNS embryonal tumor	5/5 (100%)	0/5 (0%)	2/5 (40%)	3/5 (60%)
CPT	11/11 (100%)	2/11 (18%)	7/11 (64%)	2/11 (18%)
Meningioma	16/16 (100%)	1/16 (6%)	4/16 (25%)	11/16 (69%)
Craniopharyngioma	13/13 (100%)	1/13 (8%)	2/13 (15%)	10/13 (77%)
Neuronal/glial mixed	28/28 (100%)	17/28 (61%)	6/28 (21%)	5/28 (18%)
Glioma	69/80 (86%)	26/80 (33%)	30/80 (37%)	13/80 (16%)
•Pilocytic astrocytoma, grade I	20/27 (74%)	13/27 (48%)	6/27 (22%)	1/27 (4%)
•Piloxyoid/pilocytic astrocytoma, grade II	2/2 (100%)	2/2 (100%)	0/2 (0%)	0/2 (0%)
•Fibrillary/diffuse astrocytoma, grade II	7/8 (88%)	4/8 (50%)	3/8 (38%)	0/8 (0%)
•Oligodendrogliomas, grade II	5/5 (100%)	2/5 (40%)	2/5 (40%)	1/5 (20%)
•Anaplastic astrocytoma, grade III	0/2 (100%)	0/2 (100%)	0/2 (100%)	0/2 (100%)
•Glioblastoma, grade IV	15/15 (100%)	2/15 (13%)	5/15 (33%)	8/15 (53%)
•DIPG	20/21 (95%)	3/21 (14%)	14/21 (67%)	3/21 (14%)

CNS, central nervous system; CPT, choroid plexus tumor; DIPG, diffuse intrinsic pontine glioma.

specimens on TMAs were scored microscopically by a board-certified neuropathologist (D.J.P.). Based on the histopathological assessment of the average staining intensity in at least 50% of tumor cells, tissue cores were initially scored on a 5-point scale which was then consolidated into a 3-point semiquantitative score as follows: negative (0), low (1), medium (2, 3), or high (4, 5) staining intensity.

Staining concentration was additionally quantitatively analyzed in an automated fashion using Fiji/ImageJ software (NIH, Bethesda, MD) by another investigator (S.M.). The file was grayscale (8-bit), blurred (Gaussian blur with $\sigma = 2$), thresholded, and masked to measure the total tissue surface area. The same original images were also color-deconvoluted, and DAB-staining files were blurred (Gaussian blur with $\sigma = 2$), thresholded, and masked to measure DAB-positive surface area. Staining concentration was defined as the ratio between DAB-positive and total tumor area in each file.

Good correlation was observed between the two quantification methods, with an increase in staining intensity (pathological score) associated with staining concentration (image analysis) (Supplementary Fig. 1).

B7–H3 mRNA Expression Status and Survival Analysis in Patients

We assessed B7–H3 mRNA expression status and association with overall survival in various pediatric CNS tumor types by curating publicly available patient gene expression data sets derived from the bioinformatics analysis and visualization platform GlioVis (gliovis.bioinfo.cnio.es). The patient gene expression data sets and Gene Expression Omnibus (GEO) identifiers used are as follows: pediatric medulloblastoma – Cavalli (sample size $n = 763$; GEO ID: gse85217) [27]; pediatric glioma – Paugh (sample size $n = 53$; GEO ID: gse19578) [28]; and pediatric ependymoma – Hoffman (sample size $n = 65$; GEO ID: gse50385) [29]. Association of B7–H3 expression to overall survival was estimated using a median or mean cutoff provided on the GlioVis platform to separate high (red) and low (blue) expressing patient groups.

Statistical Analysis

To investigate the associations of tumor B7–H3 expression with different clinicopathological factors, statistical analyses were conducted using one-way analysis of variance (ANOVA) and Tukey's multiple comparison. Differences between groups were considered to be significant at a p -value of < 0.05 . Statistical analyses were performed using GraphPad Prism, version 7.0 and following versions (GraphPad Software, Inc., San Diego, CA). The overall survival based on mRNA B7–H3 expression status (high or low) comparison in patients is performed using the standard univariate log-rank test, and a p -value ≤ 0.05 was considered statistically significant. Data are represented in box plots showing the minimum to maximum distribution.

Results

B7–H3 Expression in Pediatric CNS Tumors

We analyzed the expression of B7–H3 by immunohistochemistry using TMAs containing a diversity of pediatric CNS tumors. We found that expression levels were highly variable across and within tumor types, with some samples having minimal B7–H3 expression and others having an almost universal expression pattern, with staining concentrations close to 1.0 (i.e., the entire sample was positive for B7–H3). When analyzed against nontumoral brain tissue that

included both the cortex and cerebellum (Figure 1A), atypical teratoid rhabdoid tumors (ATRTs) ($p < 0.0001$, Figure 1B), ependymomas (all grades) ($p < 0.0001$, see Figure 2 for grade-by-grade analysis), medulloblastomas ($p < 0.0001$, Figure 1C), CETs ($p < 0.0001$, Figure 1D), CPTs ($p = 0.003$, Figure 1E), meningiomas ($p < 0.0001$, Figure 1F), and craniopharyngiomas ($p < 0.0001$, Figure 1G) all had higher B7–H3 staining concentrations than the normal brain. Analysis of B7–H3 mRNA expression within medulloblastoma subtypes was performed using publicly available data sets (Cavalli [27], on GlioVis); we observed significant differences in B7–H3 expression across histological (Supplementary Figure 2A) and molecular subtypes (Supplementary Figure 2B and 2C; all statistically significant except for the SHH-Group 3 pair). B7–H3 expression was highest in the Wnt subtype and lowest in the SHH subtype.

On the other hand, gliomas (including all grades, with a majority of low-grade samples) ($p = 0.3$, see Figure 2 for grade-by-grade analysis), neuronal/glial mixed tumors ($p = 0.09$, Figure 1H), and germ cell tumors ($p = 0.9$, not shown) did not differ from the normal brain in their levels of B7–H3 expression (Figure 1I).

All ATRT specimens ($n = 13$) (median age of 2.5 years) showed B7–H3 immunostaining, with 92.3% ($n = 12$) showing high and 7.6% ($n = 1$) medium staining intensities. All medulloblastoma samples ($n = 33$, median age of 6.8 years) were B7–H3 positive, with 3% ($n = 1$) having low, 45.4% ($n = 15$) medium, and 51.5% ($n = 17$) high staining intensities. Of the 5 CETs, 2 samples (40%) showed medium intensity and 3 (60%) showed high-intensity B7–H3 staining. Meningiomas ($n = 16$, median age of 17.3 years), craniopharyngiomas ($n = 13$, median age of 7 years), and CPTs ($n = 11$, median age of 8 years) all showed some degree of labeling, with a high-intensity staining intensity of 68.7%, 76.9%, and 18.1% respectively. Neuronal and mixed neuronal-glial tumors ($n = 34$, median age of 11.9 years) and germ cell tumors ($n = 3$, median age of 18.5 years) stained positive for B7–H3 with frequencies of 17.8% ($n = 5$) high, 21.4% ($n = 6$) medium, and 60.7% low ($n = 17$) staining intensities (Table 1) – overall, in these cases, there was no difference in expression from the normal brain (Figure 1I).

B7–H3 Expression Across Grade

In trying to understand the prognostic value of B7–H3 expression, we analyzed its expression across World Health Organization (WHO) grade for those tumors where this information was available. For gliomas, we observed significantly stronger staining intensity in specimens with high-grade histopathology. 53.3% of GBMs showed high-intensity B7–H3 labeling. In DIPG, 67% demonstrated medium-intensity labeling and 14% demonstrated high-intensity labeling. In contrast, grade I pilocytic astrocytomas showed low- (48%), medium- (22%), and high- (4%)-intensity B7–H3 staining of tumor specimens (Table 1). We observed that grade I ($p = 0.8$) and grade II ($p = 0.9$) gliomas did not have significantly different B7–H3 staining concentration from nontumoral brain (both the cortex and cerebellum). Grade III and IV gliomas, however, had significantly higher B7–H3 staining concentration ($p < 0.0001$) (Figure 2A and 2B), as did DIPG tumors ($p = 0.01$, Supplementary Figure 3A and 3B). The large number of low-grade samples in our cohort thus explains why the expression of B7–H3 in gliomas, as a group, is not different from that of the normal brain. Of note, the two anaplastic astrocytomas (WHO grade III) in our cohort had no B7–H3 expression. We further correlated B7–H3 mRNA expression in pediatric gliomas in publicly available datasets (Hoffman [29], on

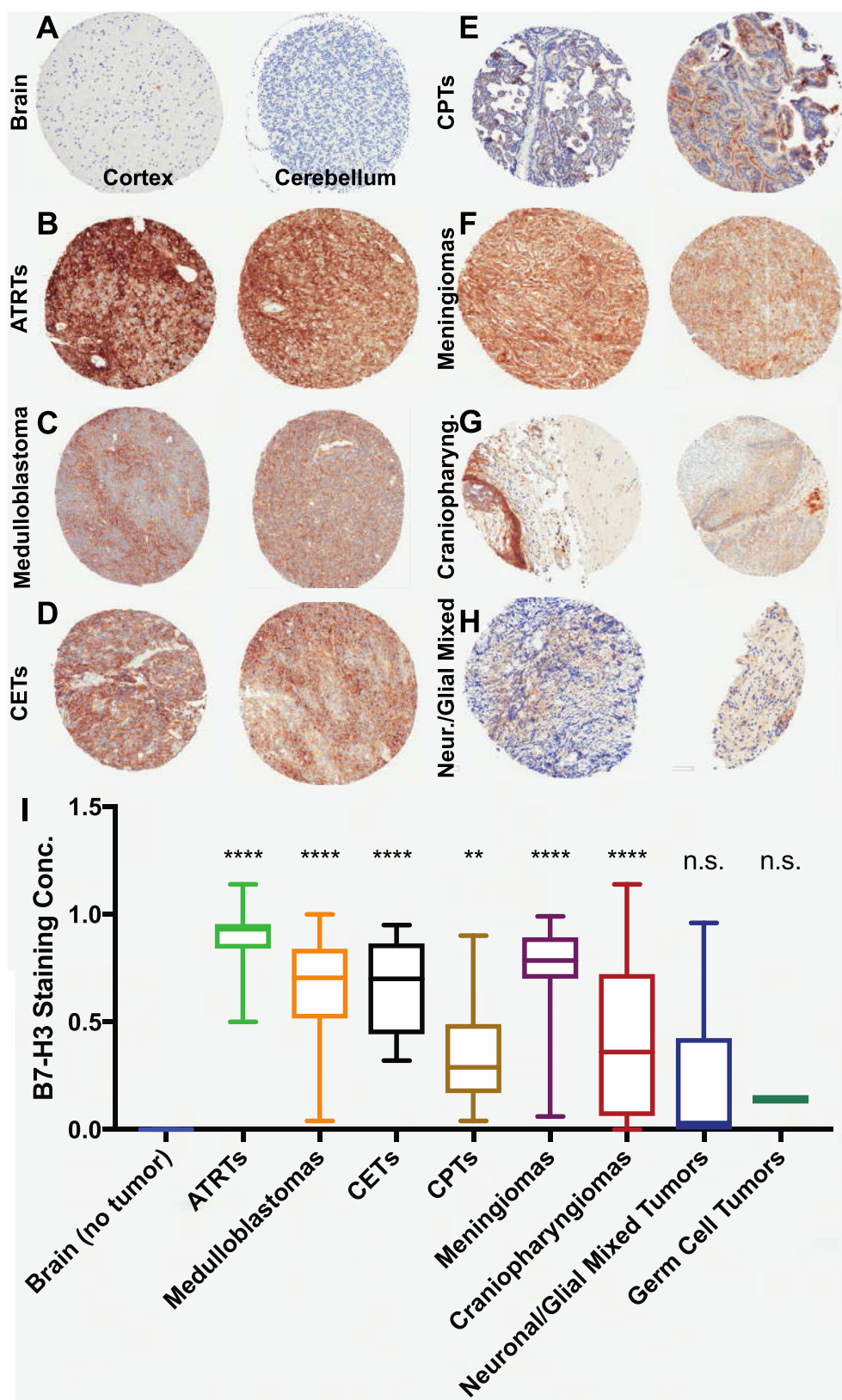


Figure 1. B7-H3 expression in pediatric brain tumors. (A–H) Representative photomicrographs of B7-H3 immunostaining of the normal brain (A), ATRTs (B), medulloblastomas (C), CETs (D), CPTs (E), meningiomas (F), craniopharyngiomas (G), and neuronal/glial mixed tumors (H). (I) Quantification of staining concentration across various tumor types against nontumoral brain samples. ATRTs, atypical teratoid rhabdoid tumors; CETs, CNS embryonal tumors; CPTs, choroid plexus tumors.

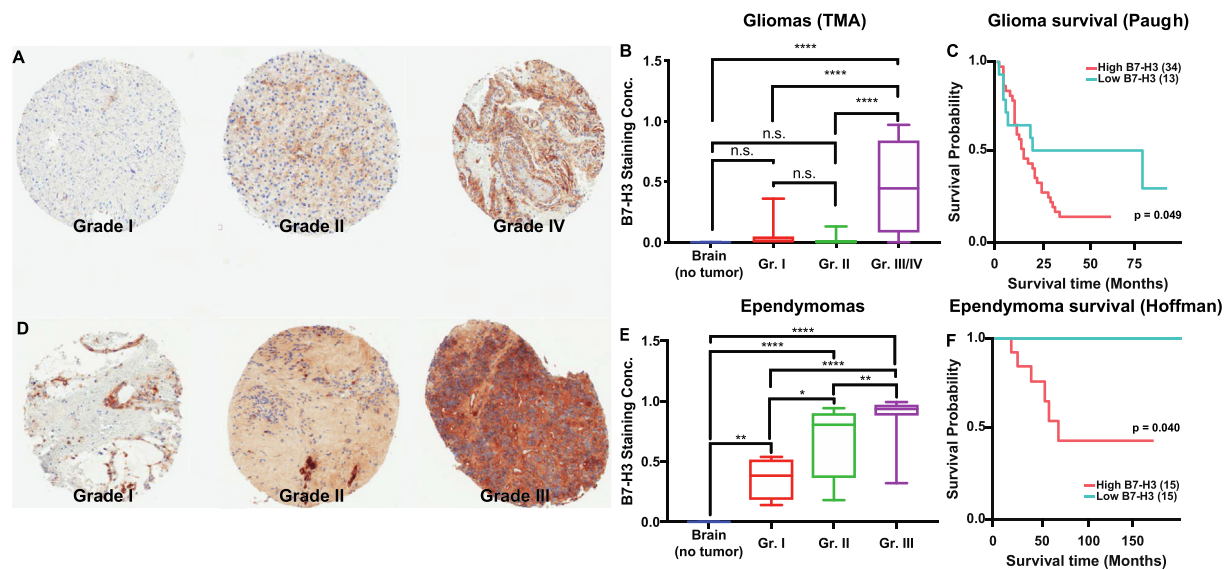


Figure 2. B7–H3 expression across WHO grade. (A) Representative photomicrographs of B7–H3 immunostaining across WHO grade for pediatric gliomas. (B) Quantification of staining concentration across WHO grades for pediatric gliomas (nontumoral brain, $n = 11$; grade I, $n = 44$; grade II, $n = 14$; grade III/IV, $n = 24$). (C) Kaplan-Meier survival curves for pediatric glioma patients (Paugh data set) divided by B7–H3 mRNA expression (high being above mean and low below mean). (D) Representative photomicrographs of B7–H3 immunostaining across WHO grade for pediatric ependymomas. (E) Quantification of staining concentration across WHO grades for pediatric ependymomas (nontumoral brain, $n = 11$; grade I, $n = 4$; grade II, $n = 10$; grade III/IV, $n = 29$). (F) Kaplan-Meier survival curves for patients with pediatric ependymoma (Hoffman data set) divided by B7–H3 mRNA expression (high being above median and low below median).

Gliosis) with survival. We noticed that B7–H3 mRNA expression above mean (“high expression,” $n = 34$, median survival = 13.2 months) was correlated with shorter overall survival when compared against “low expression” ($n = 13$, median survival = 19.2 months; $p = 0.049$, Figure 2C). Of note, the data set analyzed contains only grade III (anaplastic astrocytomas and oligodendrogliomas) and IV (glioblastoma) tumors which were found in both “high” and “low” B7–H3 expression groups, indicating how B7–H3 expression could help with survival prediction in high-grade tumors.

In ependymomas, analysis revealed that all tumors demonstrated labeling for B7–H3 staining with medium (38%, $n = 9$) or high (62%, $n = 15$) intensity (Table 1). Quantification showed increasing levels of staining concentration between grade I (myxopapillary ependymomas) and II tumors ($p = 0.05$), with grade III tumors having higher concentrations than either grade I ($p < 0.0001$) or grade II ($p = 0.005$) tumors (Figure 2D and 2E). In ependymomas, high B7–H3 mRNA expression ($n = 15$) was similarly associated with shorter median survival (61 months), regardless of grade, against low B7–H3 expression ($n = 15$; no events; $p = 0.04$, Figure 2F). Each group (“high” and “low” B7–H3 expression) consisted of seven grade II tumors and eight grade III tumors, again indicating the potential role of B7–H3 expression as an adjunct predictor. When subdivided based on location, B7–H3 staining was not different between supratentorial and infratentorial and spine ependymomas (Supplementary Figure 4A, $p = 0.09$). When publicly available mRNA data sets were analyzed with respect to molecular subtype [29], we observed how both group A and group ST ependymomas had higher B7–H3 mRNA levels than group B ependymomas (one-way ANOVA with Tukey’s multiple comparisons, $p = 0.047$ and $p = 0.017$, respectively); there was no difference between group A and group ST tumors ($p = 0.76$) (Supplementary Figure 4B).

B7–H3 Expression in Normal Human Tissues

By analyzing the normal tissue specimens which served as control specimens on the tumor TMAs, we evaluated B7–H3 immunostaining in different human tissues including the brain cortex, cerebellum, lung, muscle, tonsil, kidney, liver, gastrointestinal tract (GI), placenta, breast, prostate, and lymph nodes (Figure 3A). Analysis of staining concentrations showed a varied pattern in different human tissue types, with relatively stronger expression in the lung, liver, placenta, breast, and prostate tissues. Both the cortex and cerebellum were on the lower end of the concentration spectrum (Figure 3B). Of note, statistically significant differences were found only between the brain cortex and breast ($p = 0.006$), cerebellum and placenta ($p = 0.02$), cerebellum and breast ($p = 0.002$), muscle and placenta ($p = 0.04$), muscle and breast ($p = 0.004$), tonsils and breast ($p = 0.03$), and breast and lymph node ($p = 0.03$). Given the high variability in expression, numerous tissues had B7–H3 staining concentrations overlapping with those observed for tumor samples.

Discussion

Our group previously reported B7–H3 immunoreactivity and overexpression in DIPG and the potential for antibody-based targeted therapy against B7–H3, with a phase I clinical trial showing the safety of this approach [12,24]. However, the expression of this protein in other pediatric CNS malignancies has not been broadly investigated. To determine the potential for B7–H3 targeted agents in these malignancies, we comprehensively investigated B7–H3 protein levels in pediatric glial and nonglial CNS tumors and neuroblastomas. To our knowledge, our work provides the first large-scale evaluation of B7–H3 expression in primary CNS tumors of childhood. We show that B7–H3 protein is expressed in the vast majority of pediatric brain tumors, with high B7–H3 expression

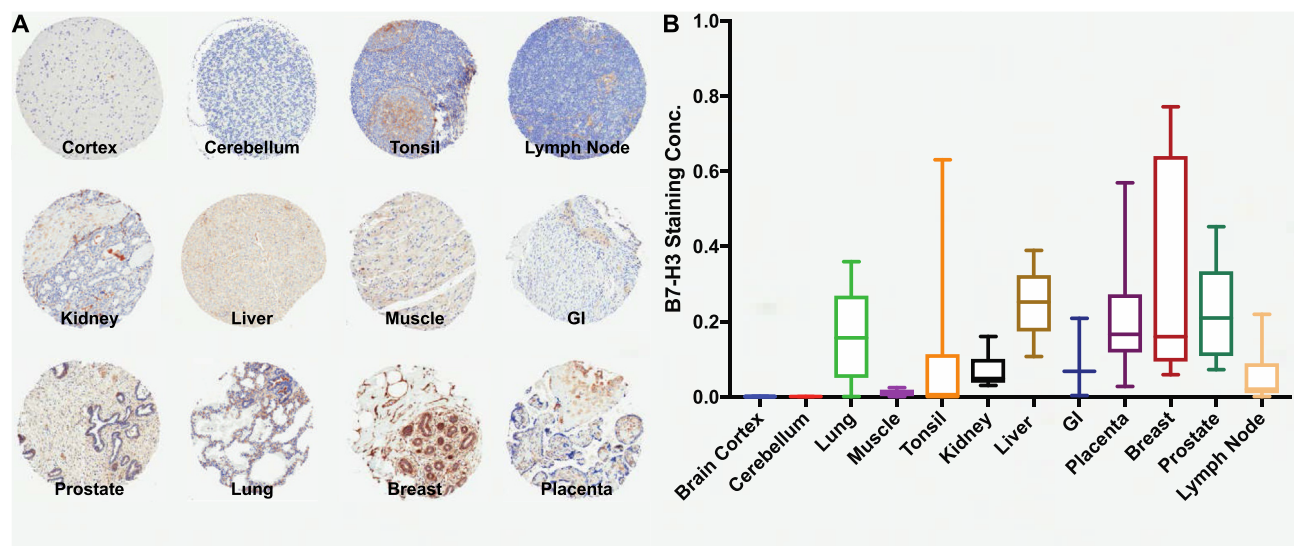


Figure 3. B7–H3 expression across nontumoral organs. (A) Representative photomicrographs of B7–H3 immunostaining of normal tissues. (B) Quantification of staining concentration in the brain cortex ($n = 5$), cerebellum ($n = 6$), lung ($n = 6$), muscle ($n = 6$), tonsil ($n = 13$), kidney ($n = 6$), liver ($n = 5$), GI ($n = 3$), placenta ($n = 56$), breast ($n = 6$), prostate ($n = 6$), and lymph node ($n = 6$).

demonstrated in a diversity of glial and nonglial tumors and particularly in high-grade tumors; ATRT tumors, a rare entity affecting young children with particularly poor prognosis [30,31], had particularly high B7–H3 expression, with all cases ($n = 13$) showing at least moderate staining and 92.3% ($n = 12$) showing a high expression level as scored by immunohistochemistry. For medulloblastomas and ependymomas, we further show differential expression across tumor grade and molecular or histological subtype.

Our results are consistent with previous studies showing aberrant overexpression of B7–H3 in both solid and hematologic malignancies [2,3,6,8,13–15,18,20,32]. Higher B7–H3 expression in human cancer tissues of hepatic, lung, pancreatic, prostate, breast, colorectal, ovarian, and various other cancers, including adult gliomas, are reported to correlate with grade, increased recurrence, and poor prognosis [1,9,11,14,16,33].

The precise role of B7–H3 activity in cancer cells has yet to be fully elucidated [6,32]. The varied expression of B7–H3 in normal tissues may be a major mechanism of physiologic peripheral immune tolerance to dampen tissue autoimmune responses. Therefore, it is important to consider immune-related adverse events to immunotherapies when targeting this antigen. However, the almost-universal high expression in tumor tissue compared with the normal brain makes B7–H3 an inviting therapeutic target. Antibodies or antibody fragments that amplify inherent immunological properties could be exploited for the killing of B7–H3-positive cancers [32,34]. These could include complement-mediated cytotoxicity (ADCC) and antibody–drug conjugate (ADC) therapies. Other more experimental approaches, such as the recruitment of cytotoxic T cells using bispecific technologies (e.g., dual-affinity retargeting [DART0 molecules or genetically reprogrammed T cells using chimeric antibody receptors (CAR-Ts)], are also in development [25,34,35]. This approach is particularly appealing for CNS malignancies, where the low B7–H3 expression observed in the normal brain parenchyma and cerebellum could potentially reduce on-target off-tumor side effects (i.e., binding to B7–H3 found outside tumor tissue). A direct drug delivery approach

could further limit overall body exposure and be even more advantageous, given the variable expression of B7–H3 in different normal organs. In fact, we have already demonstrated the safety of such an approach; direct in-tumor administration of ^{124}I –8H9, a radiolabeled monoclonal antibody against B7–H3, was recently proven safe in a phase I clinical trial in children with DIPG, with no systemic side effects directly associated with B7–H3 targeting observed [24].

In conclusion, our study demonstrates that B7–H3 protein is broadly overexpressed in pediatric glial and nonglial CNS tumors and neuroblastoma. Moreover, its expression correlates with tumor grade and prognosis in both gliomas and ependymomas. Given its tumor selectivity in the brain and the availability of targeted therapeutic agents to B7–H3, this study illustrates the potential utility of therapeutics directed to this antigen in various pediatric CNS tumors.

Conflicts of Interest

The authors have no potential conflict of interest, financial or otherwise, to disclose.

Authorship

Experimental design: UM, MMS, MS, DP, MS, CH, ND, ZZ.

Experimental implementation: UM, UT, DP, SM, DM.

Data analysis: UM, UT, CM, JV, DP, SM, DM, ZZ.

Manuscript writing and editing: UM, UT, CM, DP, SM, JV, MS, DM, ZZ, ND, CH, MMS.

Manuscript approval: all authors

Acknowledgments

This research was supported in part by the Cristian Rivera Foundation, the Olivia Bocuzzi Foundation, the Fly a Kite Foundation, the McKenna Claire Foundation, the Lyonhearted Foundation, the Christian Koehler Foundation, the Brooke Healey Foundation, the Isabella Rose Romano Foundation, the Joshua's Wish, the Lily LaRue Foundation, the Samuel Jeffers Childhood Cancer Foundation, the Ty Louis Campbell Foundation, and the Children's Brain Tumor Family Foundation.

Appendix A. Supplementary data

Supplementary data to this article can be found online at <https://doi.org/10.1016/j.tranon.2019.11.006>.

References

- [1] Xu H, Cheung IY, Guo HF and Cheung NK (2009). MicroRNA miR-29 modulates expression of immunoinhibitory molecule B7-H3: potential implications for immune based therapy of human solid tumors. *Cancer Res* **69**, 6275–6281.
- [2] Chapoval AI, Ni J, Lau JS, Wilcox RA, Flies DB, Liu D, Dong H, Sica GL, Zhu G and Tamada K, et al (2001). B7-H3: a costimulatory molecule for T cell activation and IFN-gamma production. *Nat Immunol* **2**, 269–274.
- [3] Ling V, Wu PW, Spaulding V, Kieleczawa J, Luxenberg D, Carreno BM and Collins M (2003). Duplication of primate and rodent B7-H3 immunoglobulin V- and C-like domains: divergent history of functional redundancy and exon loss. *Genomics* **82**, 365–377.
- [4] Picarda E, Ohaegbulam KC and Zang X (2016). Molecular pathways: targeting B7-H3 (CD276) for human cancer immunotherapy. *Clin Cancer Res* **22**, 3425–3431.
- [5] Sun M, Richards S, Prasad DV, Mai XM, Rudensky A and Dong C (2002). Characterization of mouse and human B7-H3 genes. *J Immunol* **168**, 6294–6297.
- [6] Hofmeyer KA, Ray A and Zang X (2008). The contrasting role of B7-H3. *Proc Natl Acad Sci U S A* **105**, 10277–10278.
- [7] Chen Y, Sun J, Zhao H, Zhu D, Zhi Q, Song S, Zhang L, He S, Kuang Y and Zhang Z, et al (2014). The coexpression and clinical significance of costimulatory molecules B7-H1, B7-H3, and B7-H4 in human pancreatic cancer. *OncoTargets Ther* **7**, 1465–1472.
- [8] Hu Y, Lv X, Wu Y, Xu J, Wang L, Chen W, Zhang W, Li J, Zhang S and Qiu H (2015). Expression of costimulatory molecule B7-H3 and its prognostic implications in human acute leukemia. *Hematology* **20**, 187–195.
- [9] Wang J, Chong KK, Nakamura Y, Nguyen L, Huang SK, Kuo C, Zhang W, Yu H, Morton DL and Hoon DS (2013). B7-H3 associated with tumor progression and epigenetic regulatory activity in cutaneous melanoma. *J Invest Dermatol* **133**, 2050–2058.
- [10] Zang X, Sullivan PS, Soslow RA, Waitz R, Reuter VE, Wilton A, Thaler HT, Arul M, Slovin SF and Wei J, et al (2010). Tumor associated endothelial expression of B7-H3 predicts survival in ovarian carcinomas. *Mod Pathol* **23**, 1104–1112.
- [11] Zang X, Thompson RH, Al-Ahmadie HA, Serio AM, Reuter VE, Eastham JA, Scardino PT, Sharma P and Allison JP (2007). B7-H3 and B7x are highly expressed in human prostate cancer and associated with disease spread and poor outcome. *Proc Natl Acad Sci U S A* **104**, 19458–19463.
- [12] Zhou Z, Luther N, Ibrahim GM, Hawkins C, Vibhakar R, Handler MH and Souweidane MM (2013). B7-H3, a potential therapeutic target, is expressed in diffuse intrinsic pontine glioma. *J Neuro Oncol* **111**, 257–264.
- [13] Ingebrigtsen VA, Boye K, Nesland JM, Nesbakken A, Flatmark K and Fodstad O (2014). B7-H3 expression in colorectal cancer: associations with clinicopathological parameters and patient outcome. *BMC Canc* **14**, 602.
- [14] Ingebrigtsen VA, Boye K, Tekle C, Nesland JM, Flatmark K and Fodstad O (2012). B7-H3 expression in colorectal cancer: nuclear localization strongly predicts poor outcome in colon cancer. *Int J Cancer* **131**, 2528–2536.
- [15] Kang FB, Wang L, Jia HC, Li D, Li HJ, Zhang YG and Sun DX (2015). B7-H3 promotes aggression and invasion of hepatocellular carcinoma by targeting epithelial-to-mesenchymal transition via JAK2/STAT3/Slug signaling pathway. *Cancer Cell Int* **15**, 45.
- [16] Tekle C, Nygren MK, Chen YW, Dybsjord I, Nesland JM, Maelandsmo GM and Fodstad O (2012). B7-H3 contributes to the metastatic capacity of melanoma cells by modulation of known metastasis-associated genes. *Int J Cancer* **130**, 2282–2290.
- [17] Kortylewski M, Jove R and Yu H (2005). Targeting STAT3 affects melanoma on multiple fronts. *Cancer Metastasis Rev* **24**, 315–327.
- [18] Baral A, Ye HX, Jiang PC, Yao Y and Mao Y (2014). B7-H3 and B7-H1 expression in cerebral spinal fluid and tumor tissue correlates with the malignancy grade of glioma patients. *Oncol Lett* **8**, 1195–1201.
- [19] Castriconi R, Dondero A, Negri F, Bellora F, Nozza P, Carnemolla B, Raso A, Moretta L, Moretta A and Bottino C (2007). Both CD133+ and CD133- medulloblastoma cell lines express ligands for triggering NK receptors and are susceptible to NK-mediated cytotoxicity. *Eur J Immunol* **37**, 3190–3196.
- [20] Gregorio A, Corrias MV, Castriconi R, Dondero A, Mosconi M, Gambini C, Moretta A, Moretta L and Bottino C (2008). Small round blue cell tumours: diagnostic and prognostic usefulness of the expression of B7-H3 surface molecule. *Histopathology* **53**, 73–80.
- [21] Takashima Y, Kawaguchi A, Hayano A and Yamanaka R (2019). CD276 and the gene signature composed of GATA3 and LGALS3 enable prognosis prediction of glioblastoma multiforme. *PLoS One* **14**:e0216825.
- [22] Wang Z, Wang Z, Zhang C, Liu X, Li G, Liu S, Sun L, Liang J, Hu H and Liu Y, et al (2018). Genetic and clinical characterization of B7-H3 (CD276) expression and epigenetic regulation in diffuse brain glioma. *Cancer Sci* **109**, 2697–2705.
- [23] Zhang C, Zhang Z, Li F, Shen Z, Qiao Y, Li L, Liu S, Song M, Zhao X and Ren F, et al (2018). Large-scale analysis reveals the specific clinical and immune features of B7-H3 in glioma. *Oncol Immunology* **7**: e1461304.
- [24] Souweidane MM, Kramer K, Pandit-Taskar N, Zhou Z, Haque S, Zanzonico P, Carrasquillo JA, Lyashchenko SK, Thakur SB and Donzelli M, et al (2018). Convection-enhanced delivery for diffuse intrinsic pontine glioma: a single-centre, dose-escalation, phase 1 trial. *Lancet Oncol* **19**, 1040–1050.
- [25] Majzner RG, Simon JS, Grosso JF, Martinez D, Pawel BR, Santi M, Merchant MS, Georger B, Hezam I and Marty V, et al (2017). Assessment of programmed death-ligand 1 expression and tumor-associated immune cells in pediatric cancer tissues. *Cancer* **123**, 3807–3815.
- [26] Bosse KR, Raman P, Zhu Z, Lane M, Martinez D, Heitzeneder S, Rathi KS, Kendsersky NM, Randall M and Donovan L, et al (2017). Identification of GPC2 as an oncoprotein and candidate immunotherapeutic target in high-risk neuroblastoma. *Cancer Cell* **32**, 295–309.e212.
- [27] Cavalli FMG, Remke M, Rampasek L, Peacock J, Shih DJH, Luu B, Garzia L, Torchia J, Nor C and Morrissy AS, et al (2017). Intertumoral heterogeneity within medulloblastoma subgroups. *Cancer Cell* **31**, 737–754.e736.
- [28] Paugh BS, Qu C, Jones C, Liu Z, Adamowicz-Brice M, Zhang J, Bax DA, Coyle B, Barrow J and Hargrave D, et al (2010). Integrated molecular genetic profiling of pediatric high-grade gliomas reveals key differences with the adult disease. *J Clin Oncol* **28**, 3061–3068.
- [29] Hoffman LM, Donson AM, Nakachi I, Griesinger AM, Birks DK, Amani V, Hemenway MS, Liu AK, Wang M and Hankinson TC, et al (2014). Molecular sub-group-specific immunophenotypic changes are associated with outcome in recurrent posterior fossa ependymoma. *Acta Neuropathol* **127**, 731–745.
- [30] Nemes K and Fruhwald MC (2018). Emerging therapeutic targets for the treatment of malignant rhabdoid tumors. *Expert Opin Ther Targets* **22**, 365–379.
- [31] Velazquez Vega JE and Brat DJ (2018). Incorporating advances in molecular Pathology into brain tumor diagnostics. *Adv Anat Pathol* **25**, 143–171.
- [32] Castellanos JR, Purvis IJ, Labak CM, Guda MR, Tsung AJ, Velpula KK and Asuthkar S (2017). B7-H3 role in the immune landscape of cancer. *Am J Clin Exp Immunol* **6**, 66–75.
- [33] Sun J, Guo YD, Li XN, Zhang YQ, Gu L, Wu PP, Bai GH and Xiao Y (2014). B7-H3 expression in breast cancer and upregulation of VEGF through gene silencing. *OncoTargets Ther* **7**, 1979–1986.
- [34] Majzner RG, Theruvath JL, Nellan A, Heitzeneder S, Cui Y, Mount CW, Rietberg SP, Linde MH, Xu P and Rota C, et al (2019). CAR T cells targeting B7-H3, a pan-cancer antigen, demonstrate potent preclinical activity against pediatric solid tumors and brain tumors. *Clin Cancer Res* **25**, 2560–2574.
- [35] Johnson S, Burke S, Huang L, Gorlatov S, Li H, Wang W, Zhang W, Tuailon N, Rainey J and Barat B, et al (2010). Effector cell recruitment with novel Fv-based dual-affinity re-targeting protein leads to potent tumor cytotoxicity and in vivo B-cell depletion. *J Mol Biol* **399**, 436–449.